Title

Mechanism of Electrolytic Reduction of SiO_2 at Liquid Zn Cathode in Molten $CaCl_2$

Authors

Yuanjia Ma[1], Akifumi Ido[2], Kouji Yasuda[2, 3, *], Rika Hagiwara[2, *], Takayuki Homma[4, *], Toshiyuki Nohira[1, *, z]

Affiliations

[1]Institute of Advanced Energy, Kyoto University, Gokasho, Uji, Kyoto 611-0011, Japan

[2]Graduate School of Energy Science, Kyoto University, Yoshida-honmachi, Sakyo-ku, Kyoto 606-8501, Japan

[3]Agency for Health, Safety and Environment, Yoshida-honmachi, Sakyo-ku, Kyoto 606-8501, Japan

[4]Faculty of Science and Engineering, Waseda University, 3-4-1 Okubo, Shinjuku-ku, Tokyo 169-8555, Japan

[*]Electrochemical Society Active Member.

[z]Corresponding author: nohira.toshiyuki.8r@kyoto-u.ac.jp

Abstract

The reaction mechanism of electrolytic reduction of SiO_2 at a liquid Zn cathode in molten $CaCl_2$ was investigated with the aim of establishing a new production process of solar-grade Si. Three types of Zn/SiO_2 contacting electrodes were prepared depending on the objectives. Cyclic voltammetry suggested two reduction mechanisms of SiO_2 at a Zn electrode. One is a direct electrolytic reduction that proceeds at potentials more negative than 1.55 V vs. Ca^{2+}/Ca. The other is an indirect reduction by liquid Ca–Zn alloy at potentials more negative than 0.85 V. The both reduction mechanisms were confirmed to proceed at 0.60 V by electrolysis and immersion experiments. Impurity analysis by ICP-AES was conducted for the Si prepared by potentiostatic electrolysis at 0.60 V, and confirmed that the concentrations of the metal elements and P were lower than the target levels for primary Si before directional solidification process.

1. Introduction

Photovoltaic (PV) power generation has attracted attention as a source of green energy that can substitute the conventional fossil-based energy. The global production of

PV cells has experienced a rapid growth in the last decade. Accordingly, their production volume increased in the 21st century by a factor of approximately 250 i.e., from 0.285 GW in 2000 to 75.5 GW in 2016. Among the many types of solar cells, crystalline Si solar cells accounted for 94.3% of the worldwide production in 2016[1]. The global production of high-purity crystalline Si also increased to 412,600 tons in 2016 i.e., by a factor of approximately 18 over the level achieved in 2000[2]. Therefore, crystalline Si solar cells would most likely remain the main product of the PV industry in the long term.

The high-purity Si used in crystalline Si solar cells is known as solar-grade Si (SOG-Si), and requires a purity of 6–7N. Approximately 90% of SOG-Si is currently produced by the Siemens process[3–5]. To develop a next-generation production process for SOG-Si, purification of metallurgical-grade Si[6–11] and metallothermic reduction of silicon halides by metal reductants[12–15] were investigated. One of the metallothermic reduction processes proposed is a reduction of $SiCl_4$ by Zn, and is known as the Du Pont process, which was the commercial process for high-purity Si production before the Siemens process was introduced[12]. There are two major advantages of the Du Pont process. One is no formation of Si–Zn intermetallic compounds due to the low chemical affinity of Zn with Si[16]. The other is the easy removal of the unreacted Zn and $ZnCl_2$

generated from the Si product because of their high vapor pressures.

For the past two decades, we have been studying the direct electrolytic reduction of solid SiO_2 to Si in molten $CaCl_2$ as a new production process of SOG-Si[17–20]. Here, since purification of SiO_2 up to 6-7N is possible at low cost[21,22], such purified SiO_2 is assumed to be used as the raw material[22]. In this process, electrochemical reduction of insulating SiO_2 is realized by using a SiO_2 contacting electrode, which provides the three-phase zone of conductor/SiO_2/$CaCl_2$[17].

$$SiO_2(s) + 4\ e^- \rightarrow Si(s) + 2\ O^{2-} \quad [1]$$

Several other research groups have also investigated the direct electrolytic reduction of SiO_2[23–34]. One of the challenges faced in the industrial application of this process is the efficient recovery and separation of the powdery Si product from unreacted SiO_2 and molten $CaCl_2$[35].

Recently, we proposed an electrolytic reduction process of SiO_2 using a liquid Zn cathode in molten $CaCl_2$. Since the electrolysis product is liquid Si–Zn alloy, its separation from unreacted SiO_2 and molten salt is expected to be easier than that entailed in the use of the conventional solid cathode[36, 37]. The choice of Zn as an alloying element stems from the very factors that render the Du Pont process advantageous, i.e., the use of Zn ensures the formation of no intermetallic compounds

with Si, and facilitates easy removal of both Zn and $ZnCl_2$. Here, the most important point is that the existence of molten salt over liquid Zn effectively suppresses the evaporation of Zn even at high temperatures such as 1123 K. Figure 1 schematically illustrates the proposed process[36, 37]. The overall process consists of three major steps: electrolysis, precipitation, and refining. In the electrolysis step, solid SiO_2 is reduced to form liquid Si–Zn alloy at a liquid Zn cathode.

$$SiO_2(s) + \text{Si–Zn } (l, \text{ low Si conc.}) + 4\ e^- \rightarrow \text{Si–Zn } (l, \text{ high Si conc.}) + 2\ O^{2-} \quad [2]$$

In the precipitation step, solid Si is recovered by lowering the temperature of the liquid Si–Zn alloy.

$$\text{Si–Zn } (l, \text{ high Si conc.}) \rightarrow \text{Si}(s) + \text{Si–Zn } (l, \text{ low Si conc.}) \quad [3]$$

Since the solubility of Si in liquid Zn is 6 at.% at 1123 K and 1 at.% at 923 K[38], 5 at.% of solid Si with reference to Zn is theoretically recovered when the temperature is lowered from 1123 K to 923 K. After the precipitation step, the Si–Zn alloy with a low concentration of Si is reused as the cathode in the electrolysis step. The Si recovered is then subjected to the refining step: that entails vacuum refining to remove residual Zn and directional solidification to manufacture SOG-Si ingots.

In our previous study, the suppression of evaporation of Zn metal by covering it

with molten $CaCl_2$ was confirmed at 1123 K[36, 37]. Moreover, the alloying rate between solid Si and liquid Zn was measured, and the formation of liquid Si–Zn alloy at a liquid Zn cathode was demonstrated[36, 37]. After potentiostatic electrolysis at 0.9 V, Si particles of sizes in the range 2–30 μm were precipitated in the solidified Zn matrix. The formation of liquid Ca–Zn alloy (reaction [4]) was also suggested by cyclic voltammetry.

$$Zn(l) + Ca^{2+} + 2\ e^{-} \rightarrow Ca\text{–}Zn(l) \quad [4]$$

Based on these results, the electrolytic reduction of SiO_2 at a liquid Zn cathode was considered to be a mixed mechanism of (A) direct electrolytic reduction of SiO_2 (reaction [5]), and (B) indirect reduction of SiO_2 by liquid Ca–Zn alloy (reaction [6]).

$$SiO_2(s) + Zn(l) + 4\ e^{-} \rightarrow Si\text{–}Zn(l) + 2\ O^{2-} \quad [5]$$

$$SiO_2(s) + Ca\text{–}Zn(l) \rightarrow Si\text{–}Zn(l) + 2\ CaO(l) \quad [6]$$

However, the evidence of (B) i.e., indirect reduction was not seen, and the contributions of (A) and (B) were not investigated.

In the present study, a series of electrolysis and immersion experiments were conducted to confirm the indirect reduction of SiO_2. Based on the results, the mixed reduction mechanism was discussed in terms of reduction rate. Finally, impurity analysis was performed for the Si particles produced at the Zn cathode.

2. Experimental

All experiments were performed in a dry Ar atmosphere at 1123 K. An Ag^+/Ag electrode was used as the reference electrode in the experiments. The experimental conditions for (a) cyclic voltammetry, (b) electrolytic reduction of SiO_2 plates, and (c) electrolytic reduction of SiO_2 particles are described below.

(a) Cyclic Voltammetry

Figure 2 shows a schematic illustration of the electrolysis cell for the observation of the reduction behavior of SiO_2 at a liquid Zn cathode. Figure 3(a) schematically illustrates the structure of the liquid Zn working electrode for cyclic voltammetry. Approximately 70 g of Zn (Wako Pure Chemical Corp., reagent grade, granule) was charged into a small Al_2O_3 crucible (AS ONE, o.d. 45 mm × height 36 mm, >99%). The small Al_2O_3 crucible was placed at the bottom of another Al_2O_3 crucible (AS ONE, o.d. 90 mm × i.d. 80 mm × height 140 mm, >99%), and approximately 500 g of $CaCl_2$ (Kojundo Chemical Laboratory Co., Ltd., >99%) was charged. A W wire (The Nilaco Corporation, diameter 2.0 mm, 99.95%) threaded into an Al_2O_3 tube (Nikkato Corp., SSA-S grade, o.d. 6.0 mm × i.d. 4.0 mm) or a SiO_2 tube (Soei Riken Corp., o.d.

120 6.0 mm × i.d. 2.0 mm) was used as the current lead and immersed in the liquid Zn in the
121 small Al_2O_3 crucible. The direct electrolytic reduction of SiO_2 occurs at the three-phase
122 interface of (Al_2O_3 or SiO_2)/$CaCl_2$ (l)/Zn (l), as shown in Fig. 3(a). For comparison, a
123 square-shaped plate of single-crystal Si (ca. 30 mm × 5 mm × 0.5 mm, p-type, (100),
124 1.5–3.0 × 10^{-3} Ω cm at 298 K) was also used as the working electrode. The counter
125 electrode was a square graphite bar (Toyo Tanso Co., Ltd., 5 mm × 5 mm × height 50
126 mm).
127
128 (b) Electrolytic reduction of SiO_2 plates
129 Figure 3(b) shows a schematic illustration of the liquid Zn cathode for the
130 investigation of the effect of indirect reduction of SiO_2 by liquid Ca–Zn alloy.
131 Approximately 125 g of Zn was charged into a small ZrO_2 crucible (AS ONE, ZrO_2
132 91.5%, Y_2O_3 8%, o.d. 60 mm × i.d. 52 mm × height 35 mm). The ZrO_2 crucible was
133 placed in a graphite crucible (Toyo Tanso Co., Ltd., IG-110 grade, o.d. 100 mm × i.d. 90
134 mm × height 120 mm) to which a graphite rod (Toyo Tanso Co., Ltd., IG-110 grade,
135 diameter 9 mm) was fixed using a stainless steel screw. Approximately 500 g of $CaCl_2$
136 was charged into the graphite crucible. A SiO_2 plate (Soei Riken Corp., 25 mm × 10 mm
137 × thickness 1 mm), fixed to an insulating tube of Al_2O_3 (Nikkato Corp., SSA-S grade,

138 o.d. 2.5 mm × i.d. 1.5 mm) by winding a Mo wire (The Nilaco Corporation, diameter
139 0.20 mm, 99.95%), was immersed into the liquid Zn in the small ZrO_2 crucible. The
140 counter electrode was the graphite crucible, and the graphite rod was used as the current
141 lead. The test piece prepared by electrolysis or immersion of SiO_2 plate was washed
142 with distilled water to remove the salt, and then immersed in HCl aq. (3 wt.%, prepared
143 from Fujifilm Wako Pure Chemical Corporation, reagent grade, 36 wt.%) overnight to
144 dissolve the Zn metal on the surface of the plate. An optical microscope (Thanko Inc.,
145 DILITE30) was used for surface observation, and the masses of the SiO_2 plates were
146 measured before and after the experiment.
147
148 (c) Electrolytic reduction of SiO_2 particles
149 Figure 4 schematically illustrates a cell for the electrolytic reduction of SiO_2
150 particles. A total of 335 g of Zn and 349 g of $CaCl_2$ were charged into an Al_2O_3 crucible.
151 After the temperature was raised to 1123 K, a total of 16.2 g of SiO_2 particles (Kojundo
152 Chemical Laboratory Co., Ltd., 0.25−1.00 mm, 99.995%) was charged into molten salt
153 uniformly using a quartz funnel. The SiO_2 particles floated on the surface of liquid Zn in
154 molten $CaCl_2$ because the densities of liquid $CaCl_2$, solid SiO_2, and liquid Zn are 2.05 g
155 cm^{-3}, 2.2 g cm^{-3}, and 5.9 g cm^{-3}, respectively, at 1123 K. A W wire (The Nilaco

Corporation, diameter 1.0 mm, 99.95%) threaded into an alumina tube was used as the current lead for liquid Zn. The counter electrode was a graphite rod (Toyo Tanso Co., Ltd., IG-110 grade, diameter 20 mm × height 40 mm) fixed to a thinner graphite rod (Toyo Tanso Co., Ltd., IG-110 grade, diameter 9 mm × height 500 mm). The sample obtained after electrolysis was cooled from 1123 K to 773 K for 35 h, then maintained at 773 K for 10 h, and further cooled to 298 K for 5 h. The ingot of Zn metal was recovered after the removal of $CaCl_2$ by flowing water. The Zn metal ingot was dissolved in HCl aq. (20 wt.%). The particles recovered after the dissolution of HCl were further washed; they were alternately immersed in HCl aq. (10 wt.%) twice and in HF aq. (5 wt.%, prepared from Tama Chemicals Co., Ltd., AA-100 grade, 38 wt.%) once overnight. The analysis was conducted using X-ray diffraction (XRD, Rigaku, Ultima 4, Cu-*K*α, λ = 1.5418 Å, 40 kV, 40 mA) and inductively coupled plasma atomic emission spectroscopy (ICP-AES; AMETEK, Inc., SPECTROBLUE).

3. Result and Discussion

(a) Cyclic Voltammetry

Figure 5 shows the cyclic voltammograms at the liquid Zn (black color) and Si plate (red color) electrodes. As for the Si electrode, the cathodic and anodic current

peaks at around 1.3–1.4 V vs. Ca^{2+}/Ca correspond to the reduction of surface SiO_2 film to metallic Si and the oxidation of Si into SiO_2 layer, respectively[35, 39]. The smaller anodic current compared with the cathodic current is due to the passivation effect of the formed SiO_2 layer. The redox at 0.5 V is attributed to $CaSi_2$/Si[35, 39]. The solid and broken black lines show the voltammograms at Zn electrodes using Al_2O_3 and SiO_2 tubes, respectively. A sharp increase in cathodic current at 0.85 V is seen at both the Zn electrodes. Since the electrochemical reduction of Al_2O_3 does not occur in the potential range measured[40], the cathodic current is attributed to the formation of liquid Ca–Zn alloy, which was already confirmed by potentiostatic electrolysis at potentials more negative than 0.85 V[37]. In the case of the Zn electrode with SiO_2, the rest potential is 1.55 V, which is more positive than that of the Si plate electrode (1.47 V), and the cathodic current is observed from the rest potential in the negative scan even at potentials more positive than 1.3 V. These results suggest the formation of liquid Si–Zn alloy with Si activity lower than unity with respect to pure solid Si. The cathodic current at the Zn electrode with SiO_2 was 80 mA larger than that with Al_2O_3, which also suggests electrolytic reduction of SiO_2 (reaction [5]).

(b) Electrolytic reduction of SiO_2 plates

On the basis of the voltammetry results, potentiostatic electrolysis was first conducted at 0.60 V and then at 0.90 V. Specifically, the experiments were conducted in the following order: [A1] electrolysis at 0.90 V for 30 min, [B1] immersion for 30 min, [A2] electrolysis at 0.60 V for 30 min, and [B2] immersion for 30 min. Here, a new SiO_2 plate was used in each step. As a result, four samples, A1, B1, A2 and B2, were prepared. Since electrolysis was not conducted for the samples B1 and B2, the reduction of SiO_2 could be advanced only due to indirect reduction by liquid Ca–Zn alloy (reaction [6]). On the other hand, the reduction of the samples A1 and A2 could proceed by a mixed reduction mechanism comprising direct electrolytic reaction (reaction [5]) and indirect reduction by liquid Ca–Zn alloy.

The optical images of the samples A1, B1, A2, and B2 are shown in Figure 6. For the sample A1, which was electrolyzed at 0.90 V, a change in color from transparent i.e., no color to dark brown is observed in a portion lower than the $Zn/CaCl_2$ interface (8 mm from the bottom of the SiO_2 plate). Also, a decrease in plate thickness is clearly observed. In the case of the sample A2, which was electrolyzed at 0.60 V, the entire area below the $Zn/CaCl_2$ interface changed to dark brown in color. In this case, the plate became thinner, showing that a larger amount of the Si–Zn liquid alloy was produced. The thickness was more decreased near the three-phase interface of $Zn/SiO_2/CaCl_2$ in

comparison with the two-phase interface of Zn/SiO_2 in liquid Zn. This is explained by higher solubility and faster diffusion of O^{2-} ions in molten $CaCl_2$ compared with those in liquid Zn. As for the immersion sample B1, no dark brown part is observed, indicating no progress of indirect reduction. Concerning the sample B2, which was immersed after electrolysis at 0.60 V, the color of the immersed portion changed to dark brown. This is explained by the indirect reduction. The weight losses of the samples were 0.03 g (A1), 0.07 g (A2), 0.00 g (B1), and 0.03 g (B2).

By comparing the samples A1 and B1, it can be inferred that only the direct reduction of SiO_2 (reaction [5]) occurs at 0.90 V. On the other hand, the results for sample A2 and B2 conclude that comparable amount of reduction proceeded in the indirect reaction, i.e., reduction by liquid Ca–Zn alloy (reaction [6]), in the electrolysis at 0.60 V to the direct reduction.

(c) Electrolytic reduction of SiO_2 particles

To prepare a sample for impurity analysis, potentiostatic electrolysis of SiO_2 particles was conducted at 0.60 V for 50 h. Figure 7(a) shows a photograph of the granules recovered after the dissolution of Zn by HCl solution and the treatment of acid washing. The XRD analysis confirms that the granules are crystalline Si (Figure 7(b)).

228 The current efficiency (η) is calculated by the following equations:

$$\eta = \frac{W_{\text{act.}}}{W_{\text{theo.}}} \times 100 \quad [7]$$

$$W_{\text{theo.}} = \frac{Q}{4F} \times M_{\text{Si}} \quad [8]$$

229 where Q is the quantity of electric charge during electrolysis, F is Faraday's constant
230 (96485 C mol^{-1}), M_{Si} is the molar weight of Si (28.1 g mol^{-1}), $W_{act.}$ is the actual weight
231 of the Si recovered, and $W_{theo.}$ is the theoretical weight of Si by Faraday's law in
232 reaction [5]. From the values of $W_{act.}$ = 3.02 g and $Q = 1.48 \times 10^5$ C, η is calculated to
233 be 28%. One of the reasons for the low current efficiency is the loss during acid
234 washing. Another is the formation of liquid Ca–Zn alloy as a side reaction; a part of it
235 contributes to the indirect reduction of SiO_2 and the other remains as Ca–Zn alloy.

236 Table 1 lists the impurity contents of the Si granules after the treatment of acid
237 washing. It also lists the acceptable levels for SOG-Si[41], segregation coefficients[7], and
238 target levels for primary Si for directional solidification. For comparison, the impurity
239 contents of the Si sample obtained by solid electrolytic reduction at 0.60 V for 5 h in
240 molten $CaCl_2$ are also shown[42]. The impurity levels of the metallic elements (Al, Ca, Fe,
241 and Ti) in the Si granules meet the target levels for the primary Si that is to be further
242 purified by unidirectional solidification according to the process proposed in Figure 1.
243 The content of P is also lower than the target level for the primary Si, and this is

244 noteworthy because the removal of P from elemental Si is known to be difficult. The
245 content of B is higher than the target level, and this needs to be improved in the future.
246 Overall, a comparison between the impurity concentrations in the Si products obtained
247 by electrolysis at a liquid Zn cathode and at a solid electrode indicates that higher purity
248 is achieved by the use of the liquid Zn electrode. The main reason for the higher purity
249 is the solidification refining during the precipitation of Si from the Si–Zn alloy wherein
250 most impurities remain in the liquid Zn phase. It should be mentioned that the Ca
251 concentration is lower than the target level for the primary Si in spite of the use of
252 indirect reduction by liquid Ca–Zn at 0.60 V. Calcium is also expected to be removed to
253 the Zn phase during precipitation. Although a relatively large amount of Zn (6055
254 ppmw) remained in the Si granules, this can be easily removed in the gas phase during
255 the refining process owing to its high vapor pressure.
256
257 **4. Conclusion**
258 The reaction mechanism of electrolytic reduction of SiO_2 at a liquid Zn cathode
259 was investigated in molten $CaCl_2$ at 1123 K. Cyclic voltammetry suggested that
260 electrolytic reduction of SiO_2 started from the rest potential (1.55 V), and liquid Ca–Zn
261 alloy was formed at potentials more negative than 0.85 V. The progress of the indirect

reduction of SiO_2 by liquid Ca–Zn alloy was confirmed by electrolysis and immersion experiments. The reduction at 0.60 V proceeded by a mixed reduction mechanism of direct electrolytic reaction and indirect reduction by Ca–Zn alloy. Impurity analysis confirmed that the concentrations of the metal elements and P were lower than the target levels for primary Si. The indirect reduction of SiO_2 by liquid Ca–Zn does not increase the Ca content of the Si product because it is removed to the Zn phase during precipitation.

Acknowledgements

This study was partially supported by Core Research for Evolutionary Science and Technology (CREST) from the Japan Science and Technology Agency (JST); Grant-in-Aid for Scientific Research A, Grant Number 16H02410, from the Japan Society for the Promotion of Science (JSPS); the Kato Foundation for Promotion of Science; and The Joint Usage/Research Center for Zero Emission Energy Research (ZE28A12), Institute of Advanced Energy, Kyoto University.

References

1. *Photovoltaic Market 2017*, RTS Corp. (2017). [in Japanese]
2. *Industrial Rare Metal 2017*, Arumu Publ. Co. (2017).

3. H. Schweickert, K. Reusche and H. Gustsche, U.S. Patent 3011877, (1961).
4. H. Gutsche, U.S. Patent 3011877, (1962).
5. C. Bye and B. Ceccaroli, *Sol. Energ. Mater. Sol. C.*, **130**, 634 (2014).
6. G. Burns, J. Rabe and S. Yilmaz, PCT International Patent WO2005/061383, (2005).
7. F. A. Trumbore, *Bell Syst. Tech. J.*, **39**, 205 (1959).
8. X. Ma, T. Yoshikawa and K. Morita, *Sep. Purif. Technol.*, **125**, 264 (2014).
9. Y. Wang, X. Ma and K. Morita, *Metall. Mater. Trans. B*, **45**, 334 (2014).
10. K. Tang, S. Andersson, E. Nordstrand and M. Tangstad, *JOM*, **64**, 952 (2012).
11. K. Hanazawa, N. Yuge and Y. Kato, *Mater. Trans.*, **45**, 844 (2004).
12. D. W. Lyon, C. M. Olson and E. D. Lewis, *J. Electrochem. Soc.*, **96**, 359 (1949).
13. S. Yoshizawa, T. Hatano and S. Sakaguchi, *Kogyo Kagaku Zasshi*, **64**, 1347 (1961). [in Japanese]
14. J. M. Blocher, Jr., M. F. Browning and D. A. Seifert, DOE/JPL Report 954339-81/21 (1981).
15. A. Sanjurjo, PCT International Patent WO1983/002443, (1983).
16. T. B. Massalski, H. Okamoto, P. R. Subramanian and L. Kacprzak, *Binary Alloy Phase Diagrams, 2nd ed.*, ASM International, Metals Park, Ohio, USA (1990).
17. T. Nohira, K. Yasuda and Y. Ito, *Nat. Mater.*, **2**, 397 (2003).
18. K. Yasuda, T. Nohira, K. Amezawa, Y. H. Ogata and Y. Ito, *J. Electrochem. Soc.*, **152**, D69 (2005).
19. K. Yasuda, T. Nohira, R. Hagiwara and Y. H. Ogata, *Electrochim. Acta*, **53**, 106 (2007).
20. T. Nohira, *Yoyuen Oyobi Koon Kagaku*, **54**, 95 (2011). [in Japanese]
21. M. Bessho, Y. Fukunaka, H. Kusuda and T. Nishiyama, *Energy Fuels*, **23**, 4160 (2009).
22. T. Homma, N. Matsuo, X. Ynag, K. Yasuda, Y. Fukunaka and T. Nohira, *Electrochim. Acta*, **179**, 512 (2015).
23. X. Jin, P. Gao, D. Wang, X. Hu and G. Z. Chen, *Angew. Chem. Int. Ed.*, **43**, 733 (2004).
24. P. C. Pistorius and D. J. Fray, *J. SAIMM*, **106**, 31 (2006).
25. S. Lee, J. Hur and C. Seo, *J. Ind. Eng. Chem.*, **14**, 651 (2008).
26. J. Yang, S. Lu, S. Kan, X. Zhang and J. Du, *Chem. Commun.*, 3273 (2009).
27. E. Juzeliunas, A. Cox and D. J. Fray, *Electrochem. Commun.*, **12**, 1270 (2010).
28. W. Xiao, X. Jin, Y. Deng, D. Wang and G. Z. Chen, *J. Electroanal. Chem.*, **639**, 130 (2010).

29. E. Ergül, İ. Karakaya and M. Erdoğan, *J. Alloy. Compd.*, **509**, 899 (2011).
30. S. Cho, F. F. Fan and A. J. Bard, *Electrochim. Acta*, **65**, 57 (2012).
31. H. Nishihara, T. Suzuki, H. Itoi, B. An, S. Iwamura, R. Berenguer and T. Kyotani, *Nanoscale*, **6**, 10574 (2014).
32. S. Fang, H. Wang, J. Yang, S. Lu, B. Yu, J. Wang and C. Zhao, *Mater. Lett.*, **160**, 1 (2015).
33. S. Fang, H. Wang, J. Yang, S. Lu, B. Yu, J. Wang and C. Zhao, *Rare Metal*, **89**, 1 (2016).
34. S. Fang, H. Wang, J. Yang, S. Lu, B. Yu, J. Wang and C. Zhao, *J. Phys. Chem. Solids*, **89**, 1 (2016).
35. T. Toba, K. Yasuda, T. Nohira, X. Yang, R. Hagiwara, K. Ichitsubo, K. Masuda and T. Homma, *Electrochemistry*, **81**, 559 (2013).
36. T. Nohira, A. Ido, T. Shimao, X. Yang, K. Yasuda, R. Hagiwara and T. Homma, *ECS Trans.*, **75**, 17 (2016).
37. K. Yasuda, T. Shimao, R. Hagiwara, T. Homma and T. Nohira, *J. Electrochem. Soc.*, **164**, H5049 (2017).
38. R. W. Olensinski and G. J. Abbaschian, *Bull. Alloy Phase Diagr.*, **5**, 271 (1984).
39. K. Yasuda, T. Nohira and Y. Ito, *J. Phys. Chem. Solids*, **66**, 443 (2005).
40. H. Kadowaki, Y. Katasho, K. Yasuda and T. Nohira, *J. Electrochem. Soc.*, **165**, D83 (2018).
41. N. Yuge, M. Abe, K. Hanazawa, H. Baba, N. Nakamura, Y. Kato, Y. Sakaguchi, S. Hiwasa and F. Aratani, *Prog. Photovolt. Res. Appl.*, **9**, 203 (2001).
42. X. Yang, K. Yasuda, T. Nohira, R. Hagiwara and T. Homma, *Metall. Mater. Trans. E*, **3**, 145 (2016).

Table and Figure captions

Table 1 Impurity contents of Si granules obtained after acid leaching, and target levels for primary Si of SOG-Si. The electrolytic reduction of SiO_2 particles was conducted at 0.6 V for 50 h at a liquid Zn cathode in molten $CaCl_2$ at 1123 K.

Figure 1 Schematic drawing of SOG-Si production process using electrochemical reduction of SiO_2 powder at a liquid Si–Zn alloy cathode in molten $CaCl_2$.[36,37]

Figure 2 Schematic illustration of the electrolysis cell for observation of SiO_2 reduction behavior at liquid Zn cathode. (a) Ag^+/Ag reference electrode, (b) Ca^{2+}/Ca dynamic reference electrode on a Mo wire, (c) liquid Zn electrode with Al_2O_3/SiO_2 tube, (d) graphite counter electrode, (e) Al_2O_3 crucible, (f) molten $CaCl_2$, (g) small Al_2O_3 crucible, and (h) liquid Zn.

Figure 3 Schematic illustrations of the liquid Zn electrode for (a) cyclic voltammetry and (b) electrolytic reduction of SiO_2 plate.

Figure 4 Schematic illustration of the electrolysis cell for the electrolytic reduction of SiO_2 particles. (a) Ag^+/Ag reference electrode, (b) Ca^{2+}/Ca dynamic reference electrode on a Mo wire, (c) W lead wire, (d) graphite counter electrode, (e) Al_2O_3 crucible, (f) molten $CaCl_2$, (g) SiO_2 particle, and (h) liquid Zn.

Figure 5 Cyclic voltammograms for liquid Zn electrode with an Al_2O_3 tube or a SiO_2

tube (left axis) and for Si plate electrode (right axis) in molten $CaCl_2$ at 1123 K. Scan rate: 100 mV s^{-1}.

Figure 6 Optical images of the SiO_2 plates after electrolysis at liquid Zn electrode or immersion into liquid Zn for 30 min in molten $CaCl_2$ at 1123 K. (a) potentiostatic electrolysis at 0.9 V, (b) immersion after electrolysis (a), (c) potentiostatic electrolysis at 0.6 V, and (d) immersion after electrolysis (c).

Figure 7 (a) An optical image and (b) XRD pattern of the Si granules obtained after acid leaching of Zn ingots. The electrolytic reduction of SiO_2 particles was conducted at 0.6 V for 50 h at a liquid Zn cathode in molten $CaCl_2$ at 1123 K.

Table 1. Impurity contents of Si granules obtained after acid leaching, and target levels for primary Si of SOG-Si. The electrolytic reduction of SiO_2 particles was conducted at 0.6 V for 50 h at a liquid Zn cathode in molten $CaCl_2$ at 1123 K.

Impurity element, A	Acceptable level for SOG-Si[41], $x_{A(SOG\text{-}Si)}$ / ppmw	Segregation coefficient[7], k°_{A}	Target level for primary Si[a], $x_{A(primary)}$ / ppmw	Impurity content of Si granules by electrochemical reduction at liquid Zn cathode, x_A / ppmw[b]	Impurity content of Si by direct electrochemical reduction[42], x_A / ppmw[c]
B	0.1–0.3	0.8	0.13–0.38	1.5	2.6
P	0.03–0.04	0.35	0.086–0.4	<0.2	6.4
Al	<0.1	2×10^{-3}	<50	8	600
Ca	<0.2	1.6×10^{-3}	<125	85	5800
Fe	<0.1	8×10^{-6}	<12500	110	30
Ti	$<10^{-3}$	9×10^{-6}	<100	25	19
Zn	—[d]	—[d]	—[d]	6055	2.1

a: $x_{A(primary)} = x_{A(SOG\text{-}Si)} / k^{\circ}_{A}$

b: Analyzed by ICP-AES

c: Analyzed by glow discharge-mass spectrometry (GD-MS)

d: No data

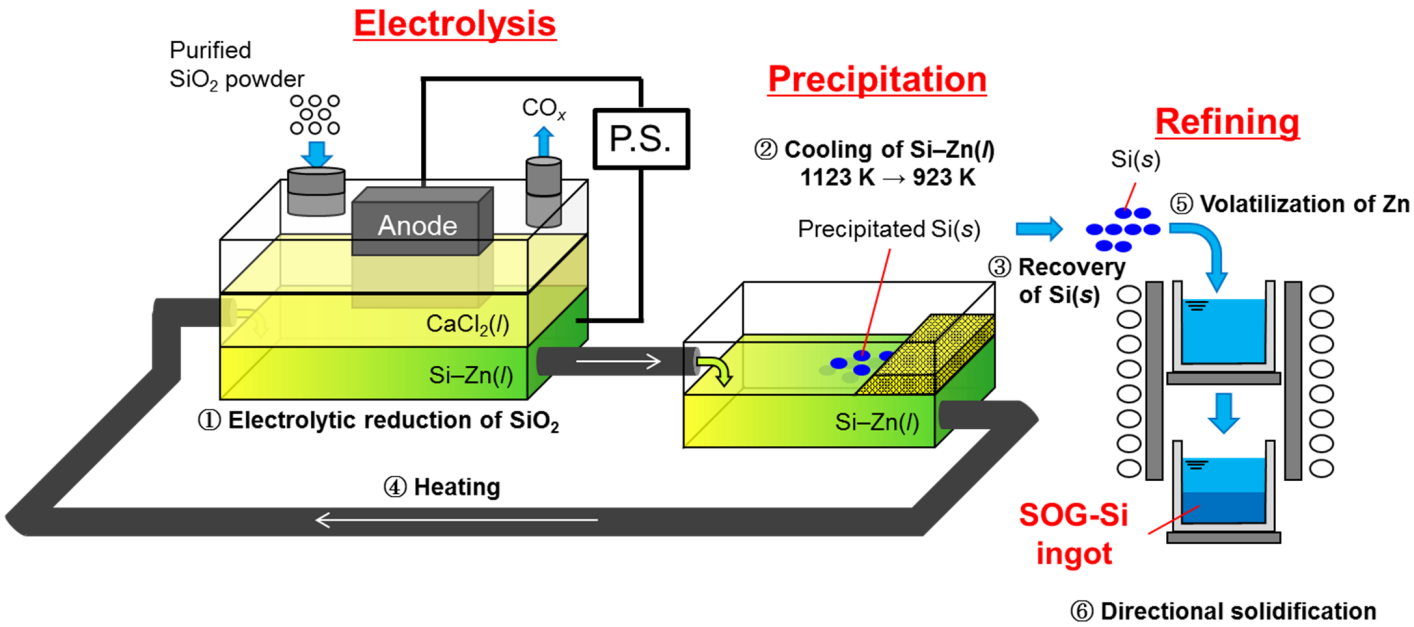

Figure 1. Schematic drawing of SOG-Si production process using electrochemical reduction of SiO_2 powder at a liquid Si–Zn alloy cathode in molten $CaCl_2$.[38]

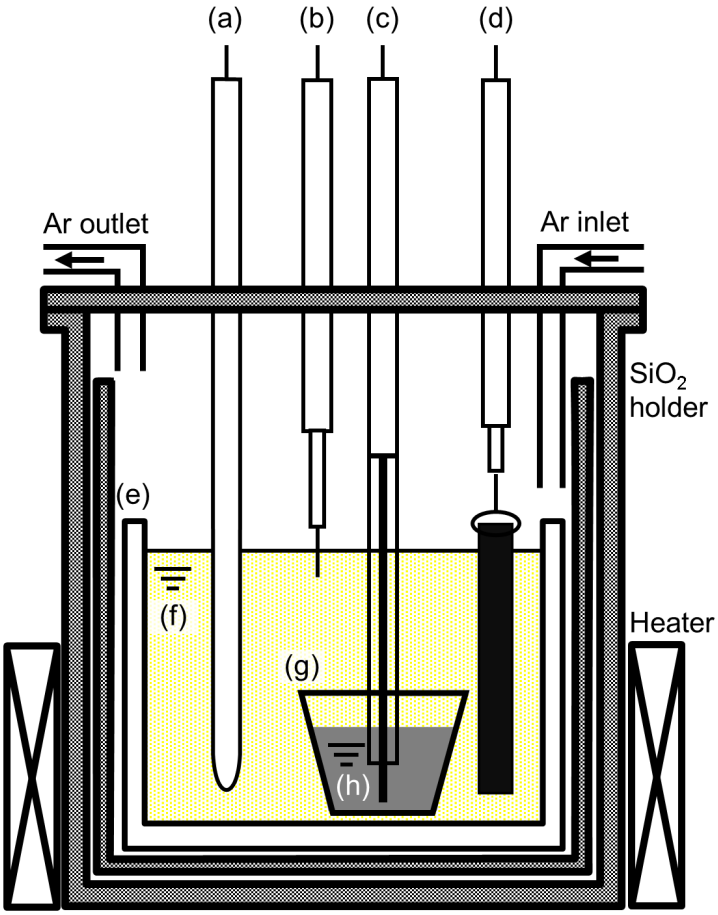

Figure 2. Schematic illustration of the electrolysis cell for observation of SiO_2 reduction behavior at liquid Zn cathode. (a) Ag^+/Ag reference electrode, (b) Ca^{2+}/Ca dynamic reference electrode on a Mo wire, (c)liquid Zn electrode with Al_2O_3/SiO_2 tube, (d) graphite counter electrode, (e) Al_2O_3 crucible, (f) molten $CaCl_2$, (g) small Al_2O_3 crucible, and (h) liquid Zn.

(a)

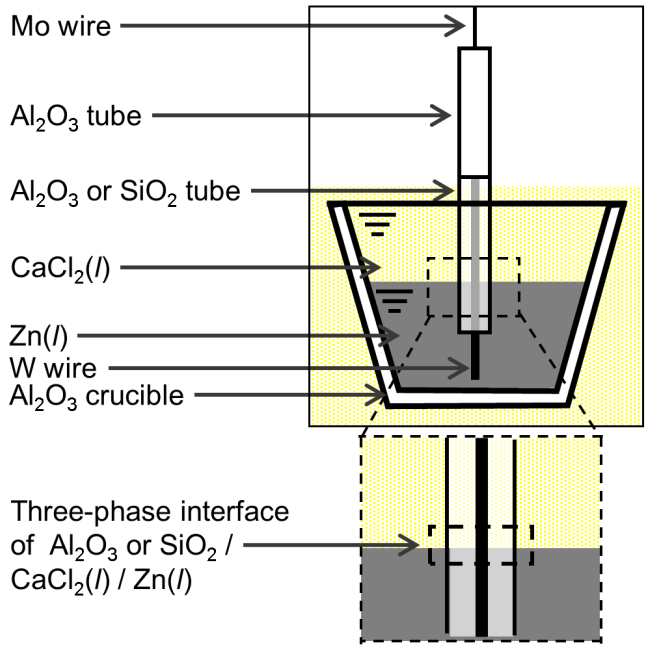

(b)

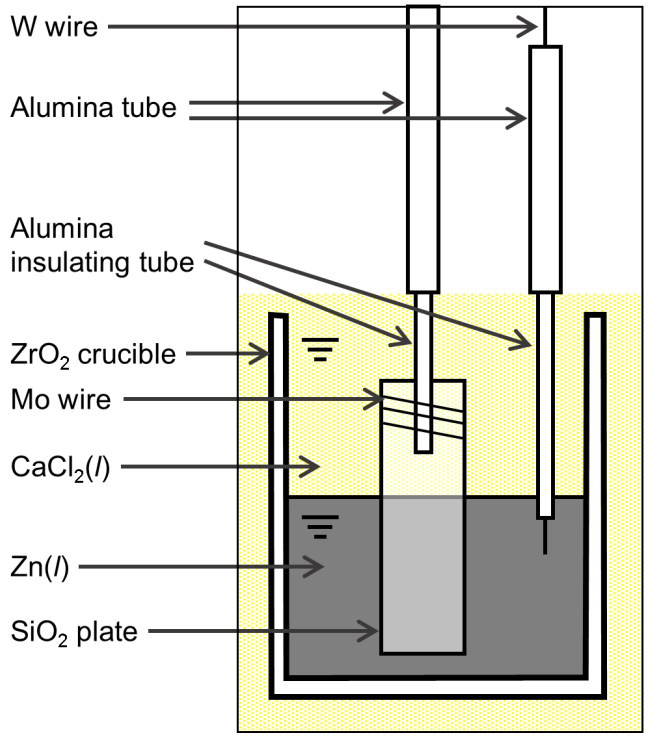

Figure 3. Schematic illustrations of the liquid Zn electrode for (a) cyclic voltammetry and (b) electrolytic reduction of SiO_2 plate

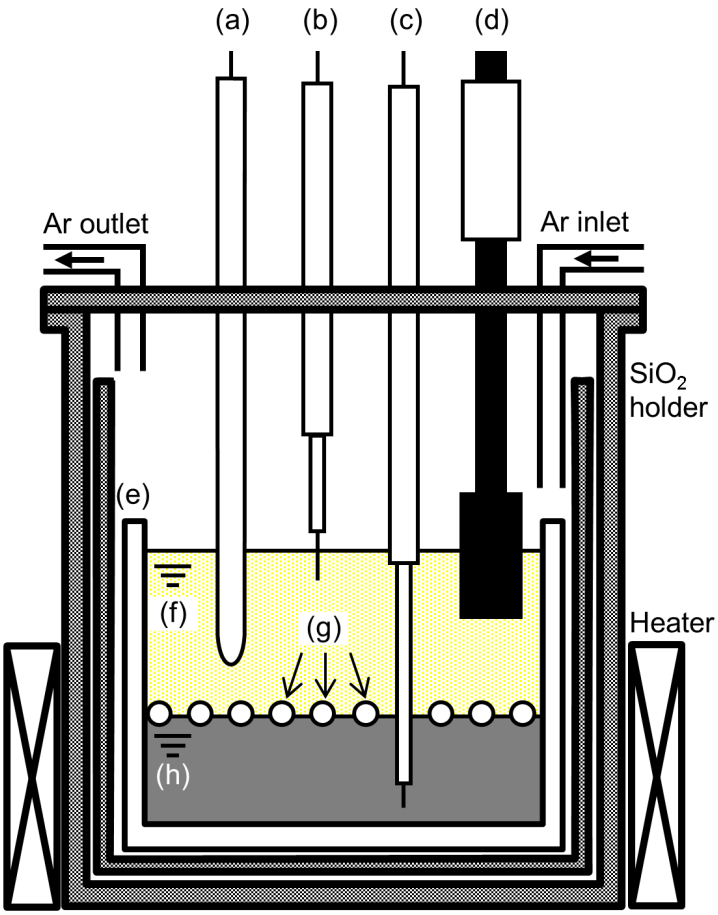

Figure 4. Schematic illustration of the electrolysis cell for the electrolytic reduction of SiO_2 particles. (a) Ag^+/Ag reference electrode, (b) Ca^{2+}/Ca dynamic reference electrode on a Mo wire, (c) W lead wire, (d) graphite counter electrode, (e) Al_2O_3 crucible, (f) molten $CaCl_2$, (g) SiO_2 particle, and (h) liquid Zn.

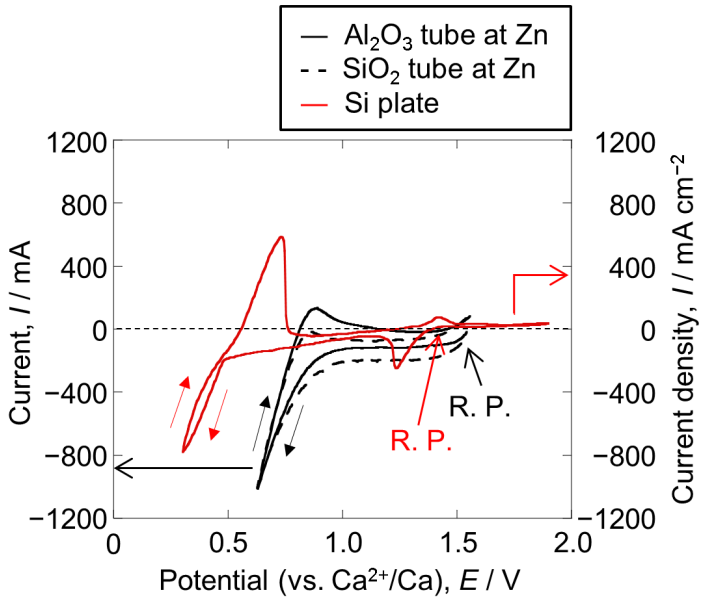

Figure 5. Cyclic voltammograms for liquid Zn electrode with an Al_2O_3 tube or a SiO_2 tube (left axis) and for Si plate electrode (right axis) in molten $CaCl_2$ at 1123 K. Scan rate: 100 mV s^{-1}.

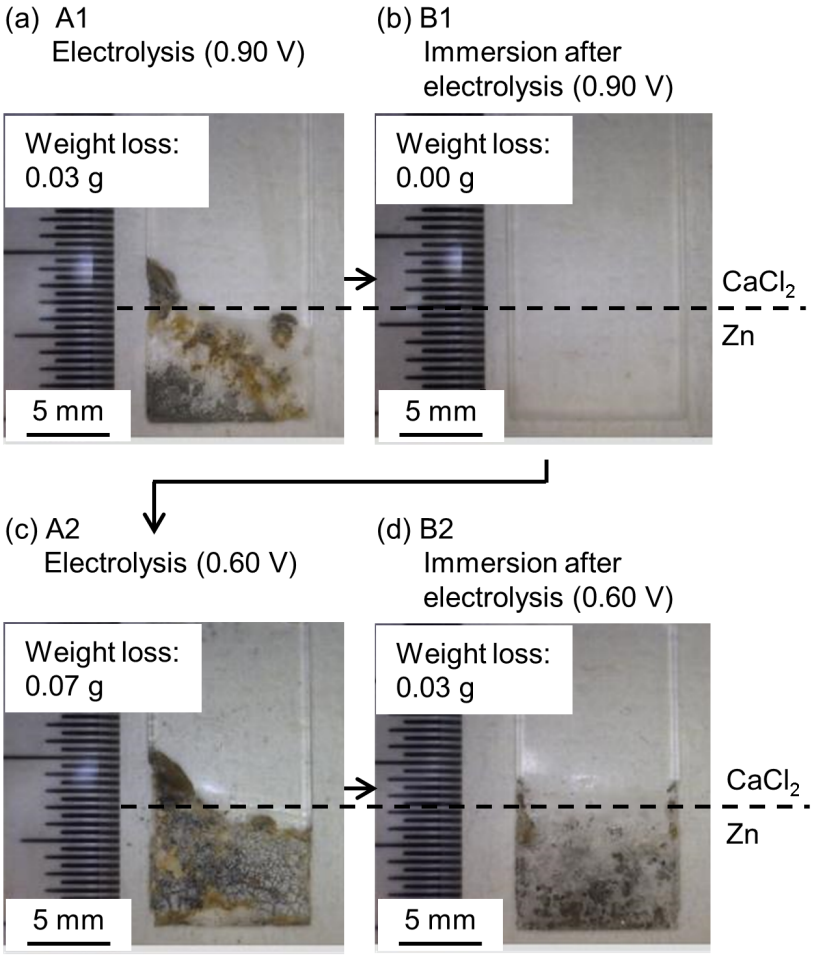

Figure 6. Optical images of the SiO_2 plates after electrolysis at liquid Zn electrode or immersion into liquid Zn for 30 min in molten $CaCl_2$ at 1123 K. (a) potentiostatic electrolysis at 0.9 V, (b) immersion after electrolysis (a), (c) potentiostatic electrolysis at 0.6 V, and (d) immersion after electrolysis (c).

(a)

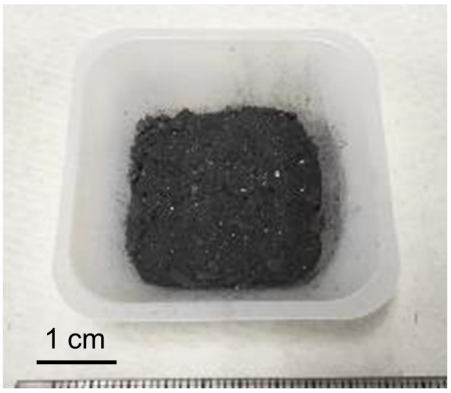

(b)

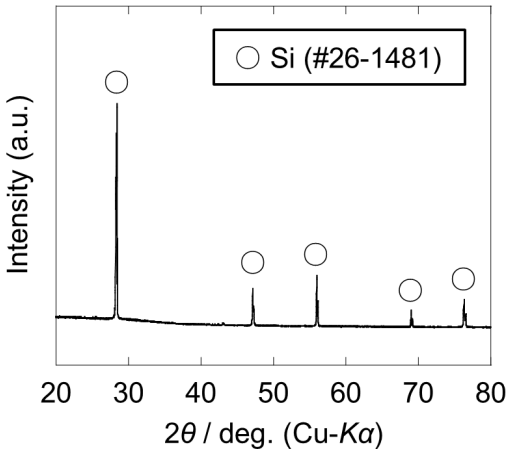

Figure 7. (a) An optical image and (b) XRD pattern of the Si granules obtained after acid leaching of Zn ingots. The electrolytic reduction of SiO_2 particles was conducted at 0.6 V for 50 h at a liquid Zn cathode in molten $CaCl_2$ at 1123 K.